Measurement of Interface Fracture Toughness of Sandwich Structures under Mixed Mode Loadings

RASMUS C. ØSTERGAARD,* BENT F. SØRENSEN AND POVL BRØNDSTED

Material Research Department, Risø National Laboratory
Frederiksborgvej 399, 4000 Roskilde, Denmark

ABSTRACT: Fracture of sandwich structures loaded with axial forces and bending moments is analyzed in the context of linear elastic fracture mechanics. A closed form expression for the energy release rate of interface cracking of a sandwich specimen is found by analytical evaluation of the *J*-integral. A method for determining the mode mixity is described and applied. Expressions are presented whereby the mode mixity can be calculated analytically for any load combination when the mode mixity is known for just one load case.

The theory presented is applied to a new test method based on double cantilever beam sandwich specimens loaded with uneven bending moments. The interface fracture toughness of two sandwich types are measured as function of the mode mixity. The sandwich structures that are tested consist of glass fiber reinforced polyester skins and PCV core. The tests show that the interface fracture toughness depends strongly on the mode mixity. Under dominated normal crack opening, the crack grows just below the interface in the core at a constant fracture toughness. Under dominated tangential crack deformation, the crack grows into the laminate resulting in extensive fiber bridging and an increase in fracture toughness. As a result of the development of a large process zone due to fiber bridging, the analysis by linear elastic fracture mechanics becomes invalid and modeling with cohesive zones is proposed.

KEY WORDS: fracture toughness, fiber bridging, energy release rate, mode mixity, LEFM.

INTRODUCTION

FRACTURE OF BRITTLE solids is often analyzed within the framework of linear elastic fracture mechanics (LEFM) which is also the most

*Author to whom correspondence should be addressed. E-mail: rasmus.c.oestergaard@risoe.dk
Figure 5 appears in color online: http://jsm.sagepub.com

1099-6362/07/05 0445–22 $10.00/0 DOI: 10.1177/1099636207070578

widespread approach for the analysis of sandwich structures. The LEFM is a convenient tool for analyzing fracture in materials and structures because analytical expressions can be derived for a wide range of practical problems. In the present work, sandwich structures with polymeric foam core and glass fiber-reinforced polymer (GFRP) skins have our primary interest. The fracture mechanisms associated with skin to core debonding will be investigated and the fracture resistance will be measured. Despite the focus on the aforementioned material combinations, the mechanics deployed in the present article are of a general character and can be used analyzing skin core debonding for sandwich structures with other material combinations.

LEFM was applied by Zenkert [1] for the analysis of skin to core debonding in sandwich structures. Carlsson and Prasad [2] conducted a study of mixed mode fracture in a specimen with isotropic material constituents where the mode mixity for different combinations of a transverse and a normal loading on the debonded sandwich skin was computed numerically. Furthermore, a comprehensive study of skin to core debonding of various types of sandwich structures was carried out by Ratcliffe and Cantwell [3], and it was found that the fracture toughness for interface debonding is in the range 170–2750 J/m^2. In the present study, LEFM for anisotropic bi-material structures [4] is used and a somewhat more general analysis is brought into context.

For cracks in interfaces between elastically dissimilar materials, the stress singularity at the crack tip is uniquely defined by the energy release rate, G and the mode mixity, ψ. A fracture criterion often applied is based on the energy release rate to be equal to a critical material value, denoted as the fracture toughness, G_c. For a crack located in an interface between two dissimilar materials, the fracture toughness can depend on the mode mixity. Liechti and Chai [5] measured the effect of the mode mixity on the fracture toughness for a crack located in a weak interface between glass and epoxy and a rise of a factor of 10 was seen for $|\psi| \to 90^\circ$ in comparison with $G_c(\psi \approx 0)$.

In the following, an analysis is carried out where the J-integral is used for calculating the energy release rate for a fairly general load situation. The load type analyzed here is rather versatile and can be applied for various practical problems. A method is then presented whereby the mode mixity can be extracted from a finite element solution of the problem. Afterwards, the mode mixity can be determined for any combination of the loads analyzed. Finally, the theory is applied to a test setup that can impose mixed mode loading to a sandwich specimen. Two types of commercially manufactured sandwich structures were tested and fracture toughness was determined as a function of mode mixity for the two. Both types had plain weave glass fiber-reinforced polyester skins. In the interface between skin

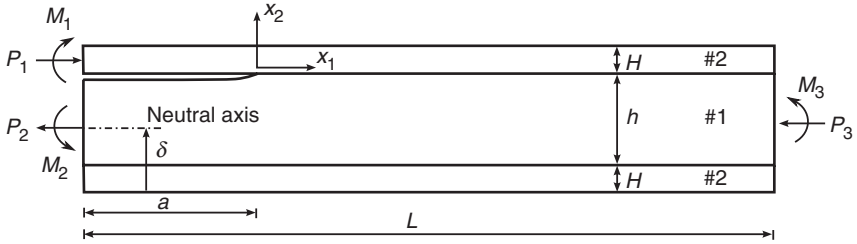

Figure 1. *Interface cracking of a sandwich with equal thickness skins is analyzed.*

and core was a layer of randomly oriented fibres (CSM). The elastic properties of the skin material were measured experimentally elsewhere [6]: $E_{11} = 14.9\,\text{GPa}$, $E_{22} = 7.53\,\text{GPa}$, $E_{33} = 16.5\,\text{GPa}$, $\nu_{13} = 0.2$, $\nu_{12} = 0.199$, $\nu_{32} = 0.16$ and $G_{12} = 2.2\,\text{GPa}$. Here, E, ν, and G are the Young's modulus, the Poisson's ratio, and the shear modulus, respectively; the subscript 1 refers to the principal material direction that is aligned with the sandwich specimen length direction (see coordinate system in Figure 1), subscript 2 denotes the out-of-plane direction and subscript 3 indicates the material axis perpendicular to 2 and 3. The fibers in the laminate plane were slightly unevenly distributed between the two principal material directions explaining the minor difference between E_{11} and E_{33}. The thickness of the sandwich skins was approximately 6 mm.

The tested sandwich structures had PVC foam core (Divinycel H80 and H130). The elastic properties of the core materials taken from [7] were used. For the H80 PVC foam, $E = 85\,\text{MPa}$, $\nu = 0.3$ and for H130, $E = 175\,\text{MPa}$, $\nu = 0.3$. The thickness of the core was approximately 40.0 mm.

In the present work we measure the fracture toughness as a function of the mode mixity. In that respect, our approach is different from the earlier studies where the fracture toughness was typically measured for only one or two mode mixities. Our approach is more information-rich and gives fracture toughness-mode mixity data that can be used as input for advanced numerical models that can account for mode mixity dependence on the fracture toughness [8].

Now, let us define a problem that is of general character and has a clear practical interest. Let the sandwich have the length L, skins of thickness H, and a core with thickness h. To keep the analysis general, the materials are considered homogeneous and orthotropic. With this choice many types of sandwich structures can be analyzed e.g., aluminium/polyvinylchloride (PVC) foam, GFRP/balsa wood, GFRP/PVC foam, etc. The isotropic behavior of some of these constituents are covered by the orthotropic description that reduces to isotropy if the elastic properties are invariant with direction. A crack with length a is located at the interface between the

core and the skin starting from the left side of the sandwich ($x_1 = -a$). The sandwich is loaded at the edges by forces per unit width, P_n, and moments per unit width, M_n, $n = 1 \ldots 3$. The problem is sketched in Figure 1.

MECHANICS OF AN INTERFACE CRACK BETWEEN TWO ELASTICALLY DISSIMILAR ORTHOTROPIC LAYERS

Material Constitutive Laws

First, let us describe the materials behavior. Both the materials are assumed to exhibit a linear elastic deformation behavior when small deformations are considered, which is reasonable for the constituents typically used in sandwich structures. The elastic deformations in the materials are described by the following relation between the stress vector, σ_i, and the strain vector, ϵ_i

$$\epsilon_i = \sum_{j=1}^{6} s'_{ij}\sigma_j, \quad i = 1 \text{ to } 6, \tag{1}$$

where

$$\epsilon_i = \epsilon_{11}, \epsilon_{22}, \epsilon_{33}, 2\epsilon_{23}, 2\epsilon_{13}, 2\epsilon_{12},$$
$$\sigma_i = \sigma_{11}, \sigma_{22}, \sigma_{33}, \sigma_{23}, \sigma_{13}, \sigma_{12},$$

and the compliance matrix s'_{ij} is given by

$$s'_{ij} = \begin{cases} s_{ij} & \text{for plane stress} \\ s_{ij} - s_{i3}s_{j3}/s_{33} & \text{for plane strain.} \end{cases}$$

The relation between the engineering constants and the compliance matrix s_{ij} can be found in appendix A.

The Singular Stress Field

Near the crack tip a singular stress field becomes dominant. The stress field in terms of the shear stress, σ_{12}, and the normal stress, σ_{22}, is given by [4]

$$\sqrt{\frac{H_{22}}{H_{11}}}\sigma_{22} + i\sigma_{12} = \frac{1}{\sqrt{2\pi}} K r^{i\epsilon - 1/2}. \tag{2}$$

Here $K = K_1 + iK_2$ is the complex stress intensity factor, $i = \sqrt{-1}$, r is the radial distance along the x_1-axis, and ϵ is the oscillatory index

$$\epsilon = \frac{1}{\sqrt{2\pi}} \ln\left(\frac{1-\beta}{1+\beta}\right),$$

where β is a generalization of the Dundurs parameter

$$\beta = \frac{\left[(s'_{11}s'_{22})^{1/2} + s'_{12}\right]_{\#1} - \left[(s'_{11}s'_{22})^{1/2} + s'_{12}\right]_{\#2}}{\sqrt{H_{11}H_{22}}}, \tag{3}$$

the parameters H_{11} and H_{22} are given in appendix B.

The crack opening components, Δu_n, are defined from the displacement u_n of two material points coinciding in the un-deformed state

$$\Delta u_n = u_n(r, \theta = \pi) - u_n(r, \theta = -\pi),$$

where the subscript n takes the values 1 and 2, that refers to the coordinate direction x_n in Figure 2. The crack opening components are related to the complex stress intensity factor, K, through

$$\sqrt{\frac{H_{11}}{H_{22}}}\Delta u_2 + i\Delta u_1 = \frac{2H_{11}}{\sqrt{2\pi}} \frac{K_r^{i\epsilon+1/2}}{(1+2i\epsilon)\cosh(\pi\epsilon)}, \tag{4}$$

and the energy release rate can be related to the complex stress intensity factor through

$$G = \frac{H_{11}}{4\cosh^2(\pi\epsilon)}|K|^2. \tag{5}$$

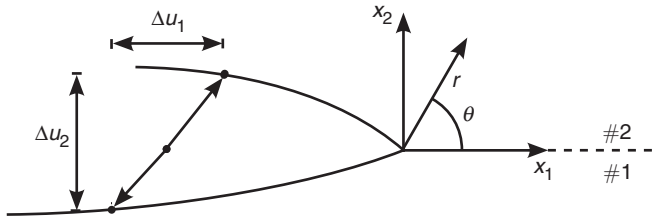

Figure 2. *Definition of crack face opening components.*

The mode mixity is defined as

$$\psi = \tan^{-1} \frac{\Im(K l^{i\epsilon})}{\Re(K l^{i\epsilon})}, \tag{6}$$

where l is a characteristic length parameter, and $\Im$ and $\Re$ are the imaginary and the real part of the complex number. The use of $l^{i\epsilon}$ in the definition of ψ is a mathematical necessity and a discussion on choosing the parameter l is elsewhere [9]. In the present work, l is set equal to the height of the core h, whereby the equations are cast in a neat form. It has been argued that l should be set equal to some characteristic length scale in the materials, e.g., the average cell diameter of the core material. One could argue that the choice of a length related to the microstructure would be more obvious in the present case, since the skin height is different from structure to structure but the microstructure of, e.g., the foam is the same [9]. On the other hand, the choice has no great importance since mode mixity calculated with $l = l_1$ can easily be recalculated to $l = l_2$ [10]. It is important to note that one implication of choosing h as the length scale is that the skin thickness of the specimen should be reported with the test results for a specific sandwich configuration.

ANALYSIS OF SANDWICH

The sandwich analyzed here is defined by the dimensions L, a, H, and h. For the subsequent derivations we ensure that the ends of the specimen, where the loads are applied, are governed by a stress field that is unaffected by stress effects from the crack tip. This can be ensured by making $(L - a)$ and a suitably long, so only the stress fields introduced by the loads M_n, P_n, $n = 1 \ldots 3$ are present at the ends of the sandwich. A finite element analysis has shown that for sandwich materials with extreme elastic mismatch $(L - a)/H > 30$ and $a/h > 1$ ensures that the stress effects from the crack do not reach the ends [11]. For the material combinations used here $(L - a)/H > 10$ and $a/h > 1$ are sufficient.

Reduced Problem

From static equilibrium it is realized that two of the six loads P_n, M_n, $n = 1 \ldots 3$ are statically determined and only four loads characterize the loading.

Since, only the stress components, σ_{12} and σ_{22}, are singular near the crack tip, the singularity is not altered if superimposing stresses in the x_1-direction.

By superimposing a stress field corresponding to an intact sandwich loaded by the moment $-M_3$ and the force $-P_3$ we arrive at a reduced problem where the singular stress components at the crack tip are as in the original problem. The superposition is illustrated in Figure 3. The relations between the reduced load parameters M and P and the original loads, P_n, M_n, $n=1\ldots3$ are

$$\begin{aligned} P &= -P_1 + C_1 P_3 + \frac{C_2 M_3}{h} \\ M &= -M_1 + C_3 M_3, \end{aligned} \tag{7}$$

where C_1, C_2, and C_3 are constants only dependent on elasticity and geometry. The constants are to be found in closed form in appendix C. This result is important since we now only have to determine the singularity in terms of G and ψ for all combinations of P and M instead of all combinations of P_n, M_n, $n=1\ldots3$.

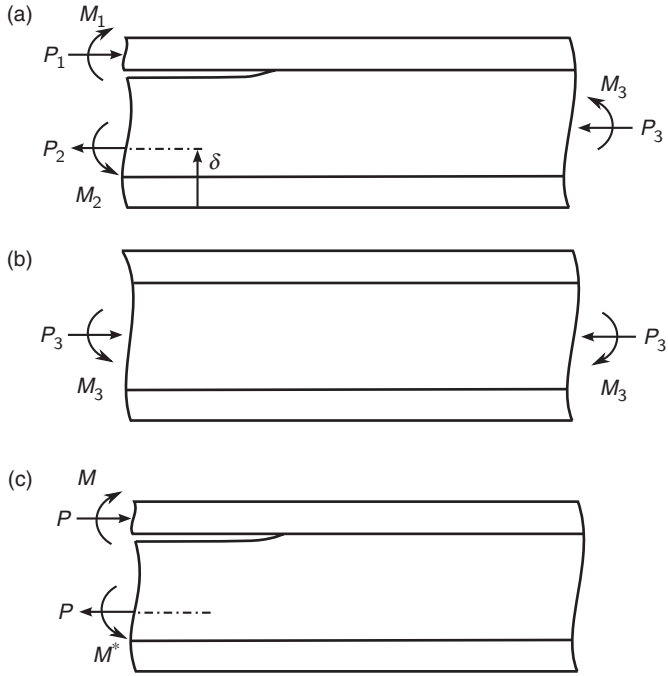

Figure 3. *By super imposing the stress field in (b) on the stress field in (a) the situation in (c) is found, where* $M^* = Ph\xi + M$ *and* ξ *is given in the appendix.*

Energy Release Rate

The energy release rate is determined by evaluating the J-integral [11] along the external boundary of the specimen. The linear elastic fracture mechanics is assumed valid and therefore $J = G$. The stresses along the boundary are needed for calculating J and they are accurately modeled by simple beam theory. Note that since the sandwich specimen is loaded only by pure moments and axial forces, there are no shear stresses in the beams and the beam slenderness condition is eliminated.

The energy release rate of the reduced problem (Figure 7c) is determined in closed form

$$G = \frac{(s'_{11})_{\#2}}{2B^2}\left(\frac{P^2}{hU} + \frac{M^2}{h^3 V} + \frac{PM}{\sqrt{UV}h^2}\sin\gamma\right), \tag{8}$$

where U, V, are γ are dimensionless constants dependent only on stiffness and geometry. They are given in appendix A. $\left(s'_{11}\right)_{\#2}$ is the compliance parameter s'_{11} for material #2, the skin material, see Equation (1). B is the width of the specimen.

The energy release rate resulting from the loadings analyzed here is independent of the crack length for a fixed load. This is the case because the specimen is a steady-state specimen, i.e., as the crack advances in a self similar fashion, the crack tip stress field merely translates along the specimen. However, this is not the case if we imagine a moment introduced by a transverse force T. Then, the moment just ahead of the crack tip would be $M = aT$ and G would be increasing for a fixed load since G would contain a factor a^2.

Mode Mixity

By combining (4), (5), (6), and (8), while setting $l = h$ the mode mixity is, upon some manipulation, expressed as

$$\tan\psi = \frac{\lambda\sin\omega - \cos(\omega+\gamma)}{\lambda\cos\omega - \sin(\omega+\gamma)}, \quad \lambda = \sqrt{\frac{V}{U}}\frac{Ph}{M}, \tag{9}$$

which is valid for $M \neq 0$. For the special case where $M = 0$ we get $\psi = \omega$. ω is a load-independent phase angle that must be determined by numerical means. ω only depends on the geometry and the compliance parameters.

However, once ω is known for one load combination, the mode mixity for any load combination can be calculated by first calculating the reduced loads according to (7) and inserting these in (9).

EXTRACTING THE MODE MIXITY FROM A FINITE ELEMENT SOLUTION

The Crack Surface Displacement Extrapolation Method

The mode mixity can only be calculated fully analytically for very simple load cases and geometries. In the general case, the mode mixity for a sandwich cannot be found analytically. Therefore, a numerical method must be deployed. In the literature several methods have been proposed for calculating the mode mixity. Suo and Hutchinson [13] were among the first to determine the mode mixity by a numerical method, however, later on more straightforward methods have been proposed [14,15]. We use a simple and yet accurate method whereby the mode mixity can be found from a finite element solution of the problem. The method is general and not restricted to the load cases introduced in Figure 1. The method we use is a crack surface displacement extrapolation (CSDE) method [8,11]. In [11], results obtained by the method were compared with results from [13] and the deviations were insignificant in the context of experimental work.

The CSDE method calculates the mode mixity, ψ, from nodal displacements along the crack faces and extrapolates the found values to the crack tip ($r \to 0$). By combining (4) and (6), it is found that ψ in radians is related to the crack surface displacements via

$$\psi = \left|_{r\to 0} \tan^{-1}\frac{\Delta u_1}{\Delta u_2} + \tan^{-1} 2\epsilon + \epsilon \ln\left(\frac{r}{l}\right), \right. \tag{10}$$

where $r \to 0$ means the value found when extrapolating to $r = 0$.

The extrapolation is performed linearly using a number of nodes in the vicinity of the crack tip. In the present work, we used nodes located in the range $H/100 < r < H/10$.

As a check of the model, G calculated from nodal displacements was compared with the G-value calculated by Equation (8), which is an exact result. By combining (4) and (5), it is found that G is related to the nodal displacements through

$$G = \left|_{r\to 0} \frac{\frac{\pi}{4}(1/2+\epsilon^2)}{rH_{11}}\left(\left(\frac{H_{11}}{H_{22}}\Delta u_2\right)^2 + \Delta u_1^2\right). \right. \tag{11}$$

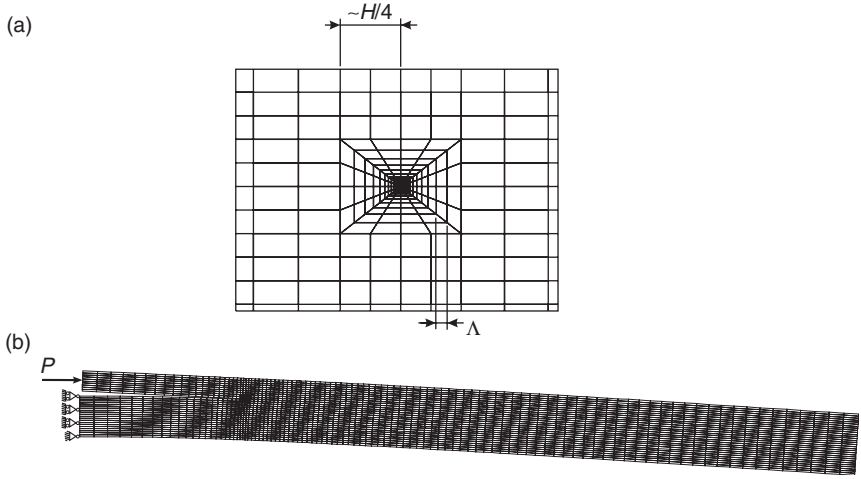

Figure 4. *Loading and mesh used for extracting the mode mixity.*

In all cases the relative deviation between numerical and analytical values was less than 0.005. Furthermore, by comparing the results with results found with meshes having significantly more elements ψ and G calculated by (10) and (11), respectively, were shown to be mesh-independent. Figure 4 shows a typical mesh used for the calculation. In order to resolve the stress and displacement field at the crack tip, the mesh was refined near the crack tip [8,11].

Extracting the Load-independent Phase Angle ω from a Load Case

As described in the section 'Mode mixity', the load-independent phase angle ω should be determined for a single load case for each sandwich structure. Using Equation (10), the mode mixity can be extracted from a finite element solution of the sandwich loaded with any combination of the loads M_n, P_n, $n = 1 \ldots 3$. A convenient choice is to take $P \neq 0$ and $M = 0$ (Figure 4). Then according (9) to $\omega = \psi$.

The following results are found from the finite element calculations with $l = h = 40.0$ mm.

Configuration	ω
GFRP/H80	60.2°
GFRP/H130	66.0°

Now, with ω determined we can analytically determine the mode mixity for any combinations of the loads M_n, P_n, $n=1\ldots3$ as follows: First, the force and moment, P and M, of the reduced problem are calculated from (7). Then, by (9), λ and ψ are calculated.

Having completed the stress analysis, we now proceed to the experimental work.

APPLYING THE THEORY TO A TEST SETUP

The theory is now applied to an experimental test setup by which the fracture toughness of sandwich structures can be measured for different mode mixities. Various test setups have been suggested for testing the fracture toughness of sandwich structures, but we think the one used here has a number of advantages that makes it preferable: (i) only one type of specimen is needed to test the whole mode mixity range; (ii) the energy release rate is determined in analytical from (8); (iii) the mode mixity can be determined analytically via (9) when the load-independent phase angle ω is determined; (iv) under fixed/constant loads the energy release rate is independent of the crack length making the measurement of G easy. The only parameters to be measured are the applied moments; it is not necessary to record the crack length to calculate G. The fact that G is independent of crack length also facilitates stable crack growth, since under 'fixed grips' the specimen unloads itself during crack propagation so that G decreases during crack growth.

The double cantilever beam sandwich specimen is loaded by uneven moments via two arms. The test setup is shown in Figure 5. The arms are loaded through a wire/roller system that is loaded by a tensile testing machine. The force, F, is the same all along the wire (apart from the neglectable resistance from the rollers), and thus the moments are calculated by $M_1 = (\pm)F\ell_1$ and $M_2 = (\pm)F\ell_2$. The magnitudes of the moments relative to each other are changed by changing the arm lengths ℓ_1 and ℓ_2. The signs of the moments are changed by rearranging the wire as shown in Figure 5(a1) and 5(a2). The un-cracked end of the specimen is supported by a roller system that provides a moment $M_3 = M_1 - M_2$. A more detailed description of the test method can be found in [16].

The length of the specimens, L, was 300 mm and the initial debond was approximately 70 mm. The sandwich specimens were initially loaded by a moment M_1 ($M_2 = 0$) supported by M_3 ($= M_1$) until the crack had grown approximately 15 mm. This procedure was used for all specimens to ensure that they had the pre-crack introduced in the same manner.

The test setup was used measuring the fracture toughness for the two sandwich types. Twelve specimens were tested for each sandwich type.

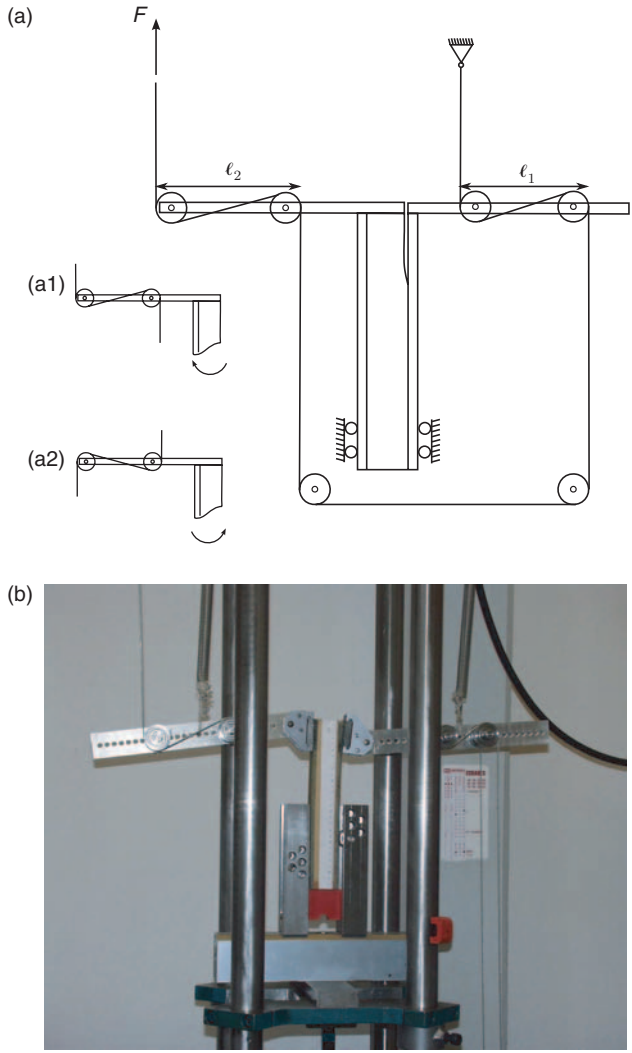

Figure 5. *(a) Sketch of the test setup. (a1) shows the arrangement of the wires that gives $M_2 > 0$ and (a2) shows the arrangement of the wires that gives $M_2 > 0$ (b) Test setup with a specimen mounted.*

The load F was measured by a 5 kN load cell and recorded on a computer with data acquisition. The tests were carried out under low displacement rate so each test had a duration of approximately 2–3 min.

The applied G was computed from the analytical expression (8) with the reduced load parameters P and M calculated from (7). Let us emphasize

that (8) and (7) are derived for a more general load situation where normal forces are applied in combination with moments. In this test method only moments are applied and we simply set the normal forces equal to zero, $P_n = 0$, $n = 1 \ldots 3$ when computing the reduced loads M and P. The mode mixity ψ was calculated by inserting the moments M_1, M_2, and M_3 $(= M_1 - M_2)$ in (7) and (9) (again with the normal forces equal to zero, $P_n = 0$, $n = 1 \ldots 3$).

TEST RESULTS

For mode mixities corresponding to deformation dominated by normal crack opening ($-35^\circ < \psi < -15^\circ$) the fracture behavior was the following: the crack initiated from the pre-crack and shifted hereafter between slow and stable growth and propagation by jumps of 10–20 mm. The crack was either in the core material or, in some cases, in the interface between skin and core. For this loading the crack grew parallel with the skin without deflecting towards the core or the skin. Schematics of the crack deformation and crack path under various load situations are shown in Figure 6.

Representative loading curves for $\psi = -30^\circ$ and -45° are shown in Figure 7. For the specimen loaded under $\psi = -30^\circ$ the load increased almost linearly with time apart from a few minor kinks that was not accompanied by any visual changes of crack length. At some critical load value, a major load drop occurred. This was accompanied by a 10–20 mm unstable crack propagation along the skin/core interface. Hereafter, the load again increased and propagation occurred at almost the same load level. Under this kind of loading the load value at each crack propagation was used as a data point and e.g., the curve for $\psi = -30^\circ$ in Figure 7 gave four data points.

When the deformation was dominated by tangential opening, corresponding to mode mixities below -35°, another behavior was observed. The crack grew into the CSM layer as sketched in Figure 6(a). Initially one to two unstable crack propagations were seen. Thereafter, a higher load level was needed to make the crack propagate. The following crack propagation was slow, stable, and the growth was accompanied by fiber bridging, i.e., fibers that were bridging from one crack face to the other. As shown in Figure 7, the load curve for $\psi = -45^\circ$ indicated a significant increase in fracture resistance (indicated by ΔP_{FB}) after the first onset of growth. Prior to fiber bridging, each point at the onset of crack growth was used as a (triangular) data point. As fiber bridging sets in, only the maximum load achieved was used as a (circular) data point. Figure 7 shows where these data points are taken from on the load curve.

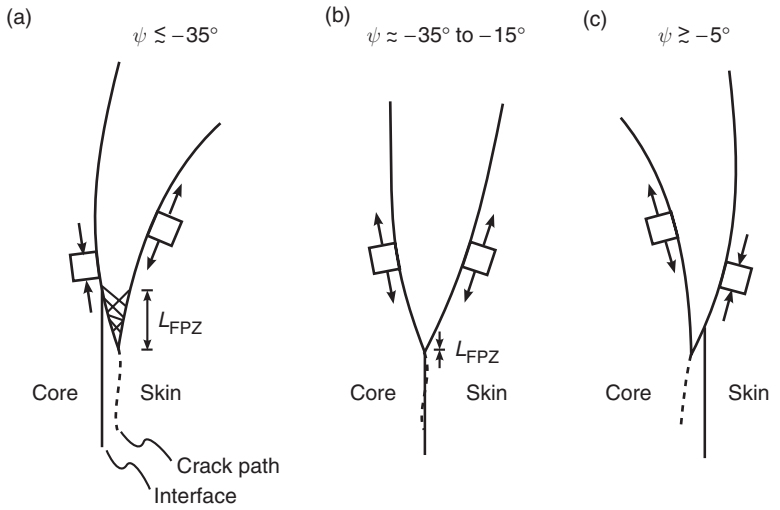

Figure 6. *Schematics of the relationship between mode mixity and crack path selection observed in the tests.*

A few test were also made with mode mixities near $-5°$, but here the crack kinked and grew at a distance into the core where it found a stable path (Figure 6(c)). For even larger mode mixities the crack deflected to the opposite side of the core. Crack kinking and stable crack paths are discussed in detail elsewhere [17], but are beyond the scope of this work.

The fracture resistance measured as a function of the mode mixity is shown in Figure 8(a) and 8(b). The left side of the graphs corresponds to a crack deformation mode where the crack is dominated by tangential displacement with a local elongation of the skin, as illustrated in Figure 6(a). The right side corresponds to a deformation mode where the crack opening is dominated by normal displacement (Figure 6(b)). The data points are segregated into two types. The triangular data points indicate applied energy release rate values at the onset of crack growth or values at crack propagation where no fiber bridging was observed from eye inspection (Figure 7). The fiber bridging mechanism will be discussed in some detail later. The data points indicated by filled circles represent maximum values of the fracture toughness in the cases where an increase in fracture resistance was seen due to e.g., fiber bridging (Figure 7). The thick line in Figure 8(a) is a numerical 'best fit' of a fourth-order polynomium to the initiation results. In Figure 8(b) second order polynomium is used for fitting. The thin lines in both figures are added 'by eye' and they show that the initiation results are spread around a band of approximately constant width.

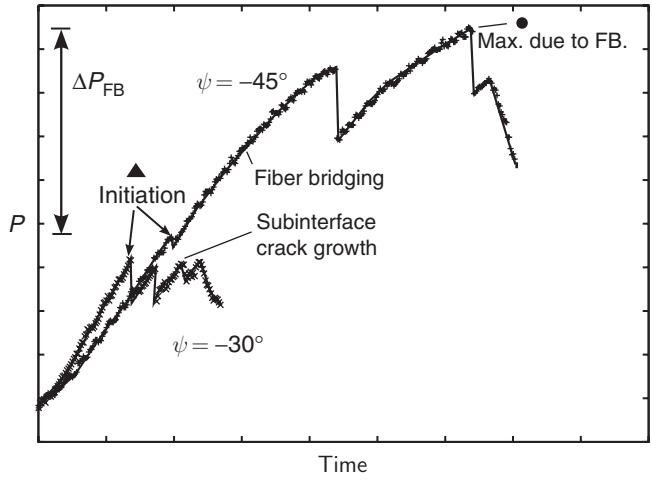

Figure 7. *Two distinctively different loading curves for tests dominated by normal opening ($\psi = -30°$) and tests dominated by tangential opening ($\psi = -45°$), respectively.*

DISCUSSION

From the measurements presented in Figure 8 it is seen that under loadings dominated by tangential crack deformation $\psi \lesssim -35°$ the maximum value of the fracture toughness is significantly higher than the initiation value. For some other loading conditions $\psi \gtrsim -35°$ no increase in fracture toughness is seen at all. To gain insight in the complex fracture behavior of the sandwich materials the subsequent section will discuss the mechanisms taking place under fracture.

When the sandwich specimen is loaded in normal crack opening, the crack grows just below the interface in the core material (Figure 9). The crack growth in the core is not associated with any noticeable increase in toughness as the crack progresses and by eye-inspection the fracture process zone seems to be small, i.e., the fracture process zone is much smaller than the skin thickness. The fact that the fracture process zone is small is important. Then, the application of LEFM is valid, since LEFM is based on the premise that length of the fracture process zone is small compared with all other geometric dimensions of the sandwich (h, H) [18]. For both types of the sandwich tested in the present study, the fracture toughness values are almost constant within the mode mixity range $-10°$ to $-30°$. For the sandwich specimen with H80 core, the applied G at crack initiation (indicated by the curve fit in Figure 8(a)) was also constant when moving further towards tangential crack opening. For the sandwich specimen

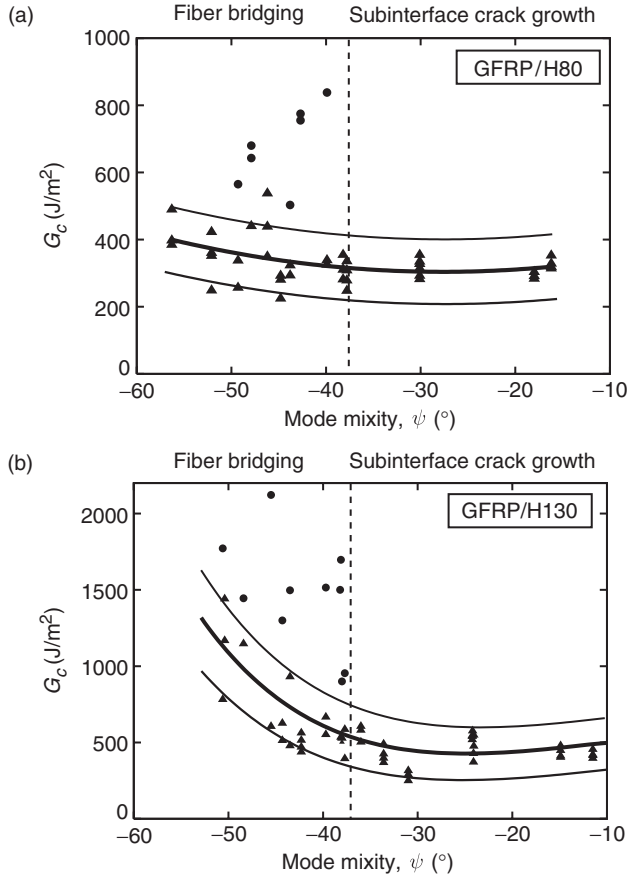

Figure 8. *The measured fracture toughness as function of mode mixity. (a) Shows the fracture toughness as function of mode mixity for the sandwich configuration with GFRP skin H80 core and (b) GFRP/H80.*

with H130, an increasing trend was apparent as applying a larger negative mode mixity. The increasing initiation toughness for H130 is a tendency also seen for other material combinations. Experimental investigations by Liechti and Chai [5] showed that for a glass/epoxy interface the toughness could increase by a factor of 10. The phenomenon has been extensively studied and Tvergaard and Hutchinson [19] showed that in an interface between elastic plastic solids the energy uptake in the plastic zone increased significantly for tangential crack deformation. Other sources for the increasing toughness is friction by asperity contact and locking near the crack tip [5,20]. The formation of the crack branches might also

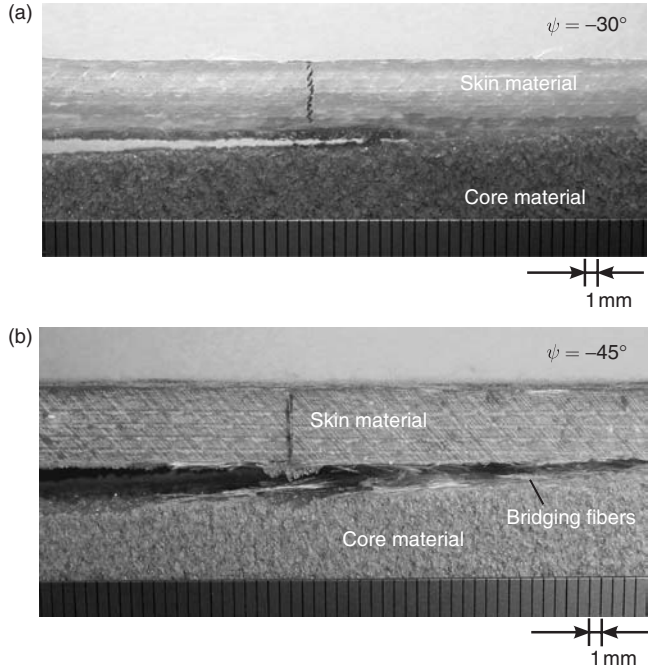

Figure 9. *(a) When the specimen has been loaded with normal crack opening, the crack grows just below the interface in the core material and (b) when the tangential crack deformation is the loading, extensive fiber bridging develops in the interface.*

explain an increased toughness. However, a detailed study to reveal which mechanisms account for the increase in toughness is beyond the scope of this work.

The observation that the crack is growing towards the skin layer for loadings giving tangential crack deformation (Figure 6(a)) can be understood from an analysis of the stresses in front of the crack tip. Under dominated normal crack opening the largest principal stress is approximately perpendicular to the interface and the crack prefers to grow just below the interface. It is well known [21] that in a homogenous material, a crack selects a mode I path, i.e., it propagates in the direction perpendicular to the largest principal stress. As the mode mixity becomes more negative, higher shear stresses arise at the crack tip. At some point the shear stresses reaches a level where crack growth in the interface becomes preferable. With a further decrease in ψ, the crack turns away from the interface and propagates into the skin laminate. The growth in the outer layer of the skin laminate leads to extensive fiber bridging and results in an increasing toughness. From Figure 9 it is clear that the length of the fracture

process zone is increasing to a length several times the skin height whereby a large scale fracture process zone is present. As mentioned, the simple LEFM is not valid for this kind of problem [18] and the results must be interpreted with caution. Fortunately, the right-hand side of (8) was derived using the *J*-integral which is also valid for large-scale bridging problems [18]. Consequently, the circular data points in Figure 8 can be interpreted as the total amount of energy dissipated per unit area in the failure process zone. However, the mode mixity loses its validity as the fracture process zone becomes longer than the zone where the singular stress field dominates. Furthermore, the fibers bridging exert forces on the crack faces and change the mode mixity.

Based on the observations here, it is clear that advanced modeling of crack growth in sandwich structures calls for more advanced modeling approaches that do not have the limitations of the LEFM e.g., cohesive zone modeling [22–24] or modeling using bridging laws and retaining a crack tip singularity [25].

The results in Figure 8(a) and 8(b) exhibit a significant spread. For initiation values the spread was in the order $200\,\mathrm{J/m^2}$. For the data points where fiber bridging was present the spread was much larger. These fracture property variations could be explained by spatial material property variation.

The literature contains many results where interfacial fracture toughness has been measured for different structures. However, the fracture toughness appears to be very sensitive to the exact choice of materials. Ratcliffe and Cantwell [3] measured the fracture toughness of a number of different configurations and found values ranging from 170 to $2750\,\mathrm{J/m^2}$. For a sandwich specimen with a H80 core, various test methods gave an average fracture toughness of approximately $270\,\mathrm{J/m^2}$. In the present study the fracture toughness values for loading under dominated normal crack opening were approximately $300\,\mathrm{J/m^2}$. The discrepancies between our results and those of Ratcliffe and Cantwell [3] are reasonably small and can be attributed to the dissimilarity in manufacture process and differences in the skin lay-up.

CONCLUSION

The test carried out in this work on sandwich double cantilever beam specimens loaded with uneven bending moments showed that the fracture toughness of sandwich structures are strongly dependent on the mode mixity. For $\psi < -35^\circ$ extensive fiber bridging results in rising fracture toughness. For the sandwich specimens tested here fiber bridges formed but a large spread in maximum toughness was seen.

For future work it is suggested that the mechanism of fiber bridging is investigated so the ability to fail by fiber bridging formation is designed into the sandwich structures since this will result in a more fracture-resistant structure.

ACKNOWLEDGEMENTS

Part of this work was part of the SaNDI (THALES JP3.23) project with participants from Norway, Denmark, Sweden, Finland, and the United Kingdom. The support of the five participating nations is gratefully acknowledged. BFS was supported by the Danish Energy Authority under the Ministry of Economics and Business Affairs through a EFP2005-fund (journal no. 33031-0078).

APPENDIX A

Relation between Compliance Matrix and Engineering Constants

Relation between engineering constants and the compliance matrices for a orthotropic and a isotropic material, respectively [26]:

$$s_{ij} = \begin{bmatrix} \frac{1}{E_{11}} & -\frac{\nu_{21}}{E_{22}} & -\frac{\nu_{31}}{E_{33}} & 0 & 0 & 0 \\ -\frac{\nu_{12}}{E_{11}} & \frac{1}{E_{22}} & -\frac{\nu_{32}}{E_{33}} & 0 & 0 & 0 \\ -\frac{\nu_{13}}{E_{11}} & -\frac{\nu_{23}}{E_{22}} & \frac{1}{E_{33}} & 0 & 0 & 0 \\ 0 & 0 & 0 & \frac{1}{G_{23}} & 0 & 0 \\ 0 & 0 & 0 & 0 & \frac{1}{G_{31}} & 0 \\ 0 & 0 & 0 & 0 & 0 & \frac{1}{G_{12}} \end{bmatrix} \tag{A1}$$

$$s_{ij} = \frac{1}{E} \begin{bmatrix} 1 & -\nu & -\nu & 0 & 0 & 0 \\ -\nu & 1 & -\nu & 0 & 0 & 0 \\ -\nu & -\nu & 1 & 0 & 0 & 0 \\ 0 & 0 & 0 & 2(1+\nu) & 0 & 0 \\ 0 & 0 & 0 & 0 & 2(1+\nu) & 0 \\ 0 & 0 & 0 & 0 & 0 & 2(1+\nu) \end{bmatrix} \tag{A2}$$

APPENDIX B

Constants for Fracture Mechanical Equations

The orthotropic materials constants $H_{11}$and H_{22} are given by

$$H_{11} = \left[2m\widehat{\lambda}^{1/4}s'_{11}s'_{22}\right]_{\#1} + \left[2m\widehat{\lambda}^{1/4}s'_{11}s'_{22}\right]_{\#2} \tag{A3}$$

and

$$H_{22} = \left[2m\widehat{\lambda}^{-1/4}s'_{11}s'_{22}\right]_{\#1} + \left[2m\widehat{\lambda}^{-1/4}s'_{11}s'_{22}\right]_{\#2}, \tag{A4}$$

where $m = \sqrt{(1+\rho)/2}$,

$$\widehat{\lambda} = \frac{s'_{11}}{s'_{22}} \tag{A5}$$

and

$$\rho = \frac{2s'_{12} + s'_{66}}{2\sqrt{s'_{11}s'_{22}}}. \tag{A6}$$

APPENDIX C

Stiffness-geometry Constants

The parameters that are used in the construction of the reduced problem are

$$\Sigma = \frac{(s'_{11})^{\#2}}{(s'_{11})^{\#1}}, \qquad \eta = \frac{h}{H}. \tag{A7}$$

Note that all the following constants only depend on these two parameters.

$$C_1 = \frac{1}{A_3\eta}, \qquad C_2 = \frac{1}{2I_3}\left(\frac{1}{\eta} + \frac{1}{\eta^2}\right), \qquad C_3 = \frac{1}{12I_3\eta^3},$$

where

$$\xi = 1 + \frac{3}{2\eta} - \Delta$$

and

$$A_1 = \frac{1}{\eta}, \qquad I_1 = \frac{1}{12\eta^3},$$

$$A_2 = \frac{1}{\eta + \Sigma}, \qquad I_2 = \frac{1}{3\eta^3} + \frac{\Delta}{\eta}\left(\Delta - \frac{1}{\eta}\right) + \Sigma\left[\left(\frac{1}{\eta} - \Delta\right)^2 + \left(\frac{1}{\eta} - \Delta\right) + \frac{1}{3}\right],$$

where

$$\Delta \equiv \frac{\delta}{h} = \frac{1 + 2\Sigma\eta + \Sigma\eta^2}{2\eta(1 + \Sigma\eta)}$$

$$A_3 = \frac{2}{\eta} + \Sigma, \qquad I_3 = \frac{2}{3\eta^3} + \frac{1}{\eta^2} + \frac{1}{2\eta} + \frac{\Sigma}{12}.$$

The parameters given in the *J*-integral solution are

$$\frac{1}{U} = \frac{1}{A_2} + \frac{1}{A_1} + \frac{\xi^2}{I_2}, \qquad \frac{1}{V} = \frac{1}{I_2} + \frac{1}{I_1}, \qquad \frac{\sin\gamma}{\sqrt{UV}} = \frac{\xi}{I_2}.$$

REFERENCES

1. Zenkert, D. (1991). Strength of Sandwich Beams with Interface Debondings, *Composite Structures*, **17**: 331–350.
2. Carlsson, L.A. and Prasad, S. (1993). Interfacial Fracture of Sandwich Beams, *Engineering Fracture Mechanics*, **44**(4): 581–590.
3. Ratcliffe, J. and Cantwell, W.J. (2001). Center Notch Flexure Sandwich Geometry for Characterizing Skin-core Adhesion in Thin-skinned Sandwich Structures, *Journal of Reinforced Plastics & Composites*, **20**(11): 945–970.
4. Suo, Z. (1989). Singularities, Interfaces and Cracks in Dissimilar Anisotropic Media, *Proc. R. Soc. Lond. A*, **427**: 331–358.
5. Liechti, K.M. and Chai, Y.S. (1992). Asymmetric Shielding in Interfacial Fracture under In-plane Shear, *Journal of Applied Mechanics*, **59**: 295–304.
6. Toftegaard, H. and Goutianos, S. (2006). Composite Skin Elastic Constants from Monolithic In-plane Specimens and Bonded Out-of-plane Specimens, *Journal of Sandwich Structures and Materials* (in press).

7. Zenkert, D. (1997). *The Handbook of Sandwich Constructions*, Engineering Materials Advisory Services Ltd., UK.
8. Berggren, C., Simonsen, B.C. and Borum, K.K. (2006). Numerical and Experimental Study of Interface Crack Propagation in Foam Cored Sandwich Beams, *Journal of Composite Materials* (in press).
9. Hutchinson, J. and Suo, Z. (1992). Mixed Mode Cracking in Layered Materials, *Advances in Applied Mechanics*, **29**: 63–191.
10. Rice, J.R. (1988). Elastic Fracture Mechanics Concepts for Interfacial Cracks, *Journal of Applied Mechanics*, **55**: 98–103.
11. Østergaard, R.C. and Sørensen, B.F. (2006). Interface Crack in Sandwich Specimens, submitted, *International Journal of Fracture*.
12. Rice, J.R. (1968). A Path-independent Integral and the Approximate Analysis of Strain Concentration by Notches and Cracks, *Journal of Applied Mechanics*, **35**: 376–386.
13. Suo, Z. and Hutchinson, J. (1990). Interface Crack between Two Elastic Layers, *International Journal of Fracture*, **43**: 1–18
14. Beuth, J. (1996). Separation of Crack Extension Modes in Orthotropic Delamination Models, *International Journal of Fracture*, **77**: 305–321.
15. Matos, P.P.L., McMeeking, R.M., Charalambides, P.G. and Drory, M.D. (1989). A Method for Calculating Stress Intensities in Bimaterial Fracture, *International Journal of Fracture*, **40**: 235–254.
16. Sørensen, B.F., Jørgensen, K., Jacobsen, T.K. and Østergaard, R.C. (2006). DCB-specimen Loaded with Uneven Bending Moments, *International Journal of Fracture*, **141**: 163–176.
17. Matteson, R.C., Carlsson, L.A., Aviles, A.V. and Loup, D.C. (2005). On Crack Extension in Foam Cored Sandwich Fracture Specimens, In: *Proceedings of the 7th International Conference on Sandwich Structures*, Aalborg University, Denmark, Springer, Dordrecht, The Netherlands.
18. Suo, Z., Bao, G. and Fan B. (1992). Delamination R-curve Phenomena due to Damage, *J. Mech. Phys. Solids*, **40**(1): 1–16.
19. Tvergaard, V. and Hutchinson, J.W. (1993). The Influence of Plasticity on Mixed Mode Interface Toughness, *J. Mech. Phys. Solids*, **41**: 1119–1135.
20. Evans, A.G. and Hutchinson, J.W. (1989). Effects of Non-planarity on the Mixed Mode Fracture Resistance of Bimaterial Interfaces, *Acta. Metall.*, **37**(3): 909–916.
21. Thouless, M.D. and Evans, A.G. (1990). Comment on the Spalling and Edge-cracking of Plates. *Scripta Metallurgica et Materialia*, **24**(8): 1507–1510.
22. Hutchinson, J.W. and Evans, A.G. (2000). Mechanics of Materials: Top Down Approaches to Fracture, *Acta Materialia*, **48**: 125–135.
23. Tvergaard, V. (1990). Effect of Fibre Debonding in a Whiskers Reinforced Metal, *Mater. Sci. Engng. A*, **125**: 203–213.
24. Jin, Z.H. and Sun, C.T. (2005). Cohesive Zone Modeling of Interface Fracture in Elastic Bi-materials, *Engineering Fracture Mechanics*, **72**(12): 1805–1817.
25. Jacobsen, T.K. and Sørensen, B.F. (2001). Mode I Intra-laminar Crack Growth in Composites – Modelling of R-curves from Measured Bridging Laws, *Composites Part A: Applied Science and Manufacturing*, **32**(1): 1–11.
26. Jones, R.M. (1975). *Mechanics of Composite Materials*, McGraw-Hill, Washington, D.C.